HHS Public Access

Author manuscript

*Mol Neurobiol*. Author manuscript; available in PMC 2022 December 06.

Published in final edited form as:

*Mol Neurobiol*. 2022 December ; 59(12): 7486–7494. doi:10.1007/s12035-022-03040-w.

# Nuclear Inhibitor of Protein Phosphatase 1 (NIPP1) Regulates CNS Tau Phosphorylation and Myelination During Development

**Cody McKee**[1], **Peter Shrager**[1], **Arindam Gosh Mazumder**[2], **Archan Ganguly**[2], **Abigail Mayer**[1], **Karl Foley**[1], **Nancy Ward**[2], **Margaret Youngman**[1], **Hailong Hou**[2], **Houhui Xia**[1,2]

[1]Neuroscience Graduate Program, Department of Neuroscience, University of Rochester Medical Center, Rochester, NY 14642, USA

[2]Department of Pharmacology and Physiology, University of Rochester Medical Center, Rochester, NY 14642, USA

## Abstract

Nuclear inhibitor of protein phosphatase 1 (NIPP1) is a known regulator of gene expression and plays roles in many physiological or pathological processes such as stem cell proliferation and skin inflammation. While NIPP1 has many regulatory roles in proliferating cells, its function in the central nervous system (CNS) has not been directly investigated. In the present study, we examined NIPP1 CNS function using a conditional knockout (cKO) mouse model in which the *Nipp1* gene is excised from neural precursor cells. These mice exhibited severe developmental impairments that led to premature lethality. To delineate the neurological changes occurring in these animals, we first assessed microtubule-associated protein tau, a known target of NIPP1 activity. We found that phosphorylation of tau is significantly enhanced in NIPP1 cKO mice. Consistent with this, we found altered AKT and PP1 activity in NIPP1 cKO mice, suggesting that increased tau phosphorylation likely results from a shift in kinase/phosphatase activity. Secondly, we observed tremors in the NIPP1 cKO mice which prompted us to explore the integrity of the myelin sheath, an integral structure for CNS function. We demonstrated that in NIPP1 cKO mice, there is a significant decrease in MBP protein expression in the cortex, along with deficits in both the conduction of compound action potentials (CAP) and the percentage of myelinated axons in the optic nerve. Our study suggests that NIPP1 in neural precursor cells regulates phosphorylation of tau and CNS myelination and may represent a novel therapeutic target for neurodegenerative diseases.

✉ Hailong Hou hlhou@live.com, Houhui Xia houhui_xia@urmc.rochester.edu.

**Author Contribution** Houhui Xia contributed to the study conception and design. Material preparation, data collection, and analysis were performed by Cody McKee, Peter Shrager, Arindam Gosh Mazumder, Archan Ganguly, Abigail Mayer, Karl Foley, Nancy Ward, Margaret Youngman, and Hailong Hou. The first draft of the manuscript was written by Houhui Xia and Cody McKee, and all authors commented on previous versions of the manuscript. All authors read and approved the final manuscript.

**Competing Interests** The authors declare no competing interests.

**Ethics Approval** All mouse experiments were performed in accordance with protocols approved by the University Committee on Animal Resources of the University of Rochester Medical Center (URMC). Our experiments comply with the ARRIVE guidelines and were carried out in accordance with the National Research Council's Guide for the Care and Use of Laboratory Animals.

**Research Involving Human Participants and/or Animals** Our research involved use of animals, but not of human subjects.

**Informed Consent** Not applicable.

**Consent to Participate** Not applicable. There are no human subjects involved in our study.

**Consent to Publish** Not applicable. There are no human subjects involved in our study.

**Keywords**

Nuclear inhibitor of protein phosphatase 1 (NIPP1); Tau; Phosphorylation; Myelination; Compound action potential (CAP); Knockout mouse

## Introduction

Nuclear inhibitor of protein phosphatase 1 (NIPP1), expressed exclusively in the nucleus, is a known regulator of protein phosphatase 1 (PP1), targeting PP1 to subnuclear localization [1]. Despite its name, PP1 complexed with NIPP1 is active in vivo [2]. Recently, NIPP1 has been shown to regulate gene expression and can interact directly with epigenetic machinery, specifically EZH2 of the polycomb repressive complex 2 (PRC2) on chromatin [3–6]. For PRC2-target genes, NIPP1 likely functions as a gene suppressor. However, many genes whose expression is regulated by NIPP1 are not PRC2-target genes [6], suggesting that NIPP1 can also regulate gene expression independently of PRC2. NIPP1 plays important roles in many physiological or pathological processes throughout the body, such as early embryonic development/cell proliferation [7], progenitor cell expansion in the adult liver [8], mammalian spermatogenesis [9], and chemokine-driven skin inflammation [10]. Recent studies suggest a role for NIPP1 in the regulation of neuronal proteins including tau [11, 12], implying a previously unexplored role for NIPP1 within the CNS.

A critical protein linked to NIPP1 activity and neurodegenerative diseases is microtubule-associated protein tau. Tau has many functions including stabilizing microtubules and facilitating fast axonal transport [13]. Tau phosphorylation is an active and crucial area of research due to the abundance of hyperphosphorylated tau in many neurodegenerative diseases including Alzheimer's disease (AD) and frontotemporal dementia with parkinsonism-17 (FTDP-17) [13]. The phosphorylation status of tau is a balance between kinases and phosphatases, including PP1 [14]. Whether nuclear inhibitor of protein phosphatase-1 (NIPP1) regulates tau phosphorylation is not yet clear.

In this report, we investigated the function of NIPP1 within the CNS by deleting *Nipp1* in embryonic neural progenitor cells (NPCs), under the nestin promoter. We found that Nestin-Cre;*nipp1*$^{fl/fl}$ (cKO) mice exhibit substantial developmental impairments and a tremor similar to that described in animals with disrupted myelination [15]. We found that there is an increase in tau phosphorylation as well as alterations in tau-associated phosphatase/kinase activation, including PP1 and AKT. Moreover, due to the presence of a tremor and poor coordination, we explored myelin structure and function in different regions of the CNS. We found that NIPP1 cKO mice show clear deficits in myelination within the brain and optic nerve as assayed by western blots, electron microscopy, and electrophysiology. In summary, our work demonstrates an important CNS function for NIPP1 in tau phosphorylation and myelination, possibly by regulating gene expression and phosphorylation signaling pathways.

## Results

We studied the potential function of NIPP1 in the CNS by deleting the *Nipp1* gene in NPCs by crossing a Nestin-Cre mouse line (Jackson Laboratories) with our floxed *Nipp1* mouse line [8]. The resulting Nestin-Cre;$Nipp1^{fl/fl}$ mouse (NIPP1 cKO) leads to embryonic knockout of the *Nipp1* gene in neurons, astrocytes, and oligodendrocytes. The mouse pups are visibly smaller than their $Nipp1^{fl/fl}$ littermate controls (Fig. 1A) and typically die prior to postnatal day (P) 30. Western blotting experiments confirmed almost complete NIPP1 protein knockout in the cortex, hippocampus, and many other brain regions (Fig. 1B). These data also suggest that NIPP1 expression by non-NPCs is minimal.

Since NIPP1 has been shown to influence tau processing in vitro, we commenced our investigation by assessing various phospho-tau epitopes. We found significant increases in tau phosphorylation, at T231 and AT8 sites (S202/T205), with a trending increase at S396, and no significant change in total tau protein level in NIPP1 cKO mice (Fig. 2). Next, we examined potential changes in the relevant tau phosphatases and kinases. We found that PP1 activity, determined from the level of the inhibitory phosphorylation at its C-terminus (pT320) [16], is significantly decreased in the hippocampus with a strong trend present in the cortex (Fig. 3A). The activity of AKT is increased in NIPP1 CKO mice as its phosphorylation at S473 is significantly increased (Fig. 3B). However, the activity of tau kinase, GSK3β, is decreased as its inhibitory phosphorylation at S9 is significantly increased (Fig. 3B).

NIPP1 cKO mice exhibited a severe tremor. Since abnormal myelination can cause a tremor, we examined the possibility of a myelination deficit in NIPP1 cKO mice. We found that myelin basic protein (MBP) expression was significantly decreased in the cortex of NIPP1 cKO mice (Fig. 4A). One possible mechanism of myelination deficit is a change in the densities of oligodendrocyte precursor cells (OPCs) and/or mature myelinating oligodendrocytes (OLs). To assess whether these populations changed in NIPP1 cKO mouse brains, we performed immunohistochemistry to measure the density of OL-lineage cells with Olig2 and ASPA antibodies (Fig. 4B, C). However, we did not observe a significant difference in pan-OL or mature OL densities within the corpus callosum denoted by Olig2 and ASPA labeling, respectively (Fig. 4B, C). In order to examine the myelin sheath directly, we performed electron microscopy (EM) on the optic nerve from NIPP1 cKO and their littermate controls (Fig. 5A). The optic nerve serves as an excellent model to study myelination due to its accessibility and its relatively high degree of myelination early in development [17]. Our data suggest no obvious difference in myelin thickness in the NIPP1 cKO mice, indicated by *g*-ratio measurements (Fig. 5B, C). Our study, however, indicates a strong deficit in the percentage of myelinated axons in the NIPP1 cKO mice (Fig. 5D). We then analyzed axon caliber, a potential mechanism to explain the myelination deficit, and found a nearly identical distribution of axon calibers (data not shown). This suggests that the myelination deficit in NIPP1 cKO mouse is not driven by an increased proportion of axons that are subthreshold in size to be myelinated.

As a further test of the influence of NIPP1 on myelination, we measured compound action potentials (CAPs) from control and NIPP1 cKO mice. At ages P14–P21, the myelinated

and un(pre)myelinated components of the CAPs from optic nerves are approximately comparable in amplitude. This preparation thus affords a sensitive test for myelin development in the CNS. The recordings show that deletion of *Nipp1* in NPCs of the CNS significantly decreased the relative myelinated component (Fig. 6A, B). However, while conduction velocity of the myelinated component was unaffected by deletion of *Nipp1*, consistent with the lack of change in *g*-ratio, surprisingly the unmyelinated fibers conducted more slowly in the cKO mice than controls (Fig. 6C, D).

## Discussion

NIPP1 is a nuclear protein regulating gene expression and has been shown to play roles in many physiological and cellular processes; however, its role in the CNS has not yet been reported. Homozygous deletion of the *Nipp1* gene is embryonic lethal and thus necessitates the need for using a conditional knockout mouse model to study brain functions. In this study, we found that the deletion of *Nipp1* from NPCs resulted in impaired development and early demise of the animal. Although a myriad of mechanisms can be involved in the animal's failure to thrive, we began our studies investigating tau and myelin, two constituents involved in numerous neurodegenerative and neurocognitive disorders. Tau hyperphosphorylation has been shown to induce microtubule destabilization, and tau mislocalization followed by aggregation, all of which can have dire consequences for neuronal function [13]. In the present study, we report increased tau phosphorylation at T231 and AT8 sites along with dysregulation of tau kinases/phosphatase activation. This is consistent with a decrease in PP1 activation and/or increased of AKT activation, known tau phosphatase and kinase, respectively. Increased phosphorylation of AKT and GSK3β, known PP1 substrates, agrees with a decrease in PP1 activity which suggests that NIPP1 could be a positive regulator of PP1. These results are reminiscent of similar effects on PP1 inhibitory phosphorylation in I-2 knockdown [16] and I-2 KO studies [18]. Additionally, we qualitatively observed gel mobility shifts in tau epitopes suggesting a possible shift in the distribution of different tau isoforms and their relative phosphorylation status. Dysregulation of tau isoforms has been demonstrated in various tauopathies [19], and the relative levels of each isoform in NIPP1 cKO mice require further investigation.

Another critical process that is abrogated in neurodegenerative diseases is myelination. Myelination of axons is important for the rapid transduction of action potentials, along with providing neurotrophic support to distal axons [20]. Not only is myelin critical for motor and sensory function but it also contributes to higher-order cognitive functions such as learning and memory [21, 22]. Dysregulation of myelination contributes to a wide range of neuropsychiatric disorders including depression and schizophrenia [23–25]. Additionally, reduced white matter has been observed in AD patients and was reported to occur even earlier than memory deficits, suggesting the possibility that CNS myelin dysfunction could contribute to AD pathogenesis.

Although OLs have an intrinsic capability to myelinate, as demonstrated when cultured with inert nanofibers [26], this process can be fine-tuned by specific neuron-OPC/OL and astrocyte-OPC/OL interactions. Specifically, neurons can modulate myelination by various mechanisms including axon caliber, secretion of trophic factors, and direct neuron-glial

synaptic transmission [27]. Neuronal activity positively regulates myelination in some regions of the CNS [28–30], possibly via regulating OPC/OL densities. However, we did not observe significant changes in OPC/OL densities in NIPP1 cKO mice. Axon caliber also does not appear to play a major role in the myelination deficit in the NIPP1 cKO mice either. PI3K-AKT-mTOR is a prominent signaling pathway important for myelination either through its action in OPC/OLs or its action in neurons, the latter of which regulates axon caliber [17, 31]. However, we did not observe a change in mTOR activation, consistent with no change in axon caliber in the NIPP1 cKO optic nerve (data not shown). On the contrary, the decrease in the percentage of myelinated axons suggests the possibility of increased axon caliber for the unmyelinated axons in the NIPP1 cKO mice. However, the conduction velocity of unmyelinated axons the NIPP1 cKO mice decreased, as opposed to an increase based on a presumed increase in axon caliber. The mechanisms of failed myelination for those axons and their slowed conduction as well as the overall myelination deficit in the NIPP1 cKO mice require further investigation.

In this report, we detected an increase in tau phosphorylation and CNS myelination deficits upon *Nipp1* deletion in the brain. Whether tau hyperphosphorylation and CNS myelination abnormalities in NIPP1 cKO mice are related is not known and needs to be studied in the future using cell-type–specific Cre lines. Finally, mechanisms underlying decreased conduction velocity in the unmyelinated component of CAPs in NIPP1 cKO also require future investigation. In summary, we have demonstrated a critical role of NIPP1 in CNS development and also imply a potential contribution in neurological disorders and diseases.

## Methods

### Mouse Model

Nestin-Cre hemizygous mice purchased from the Jackson Laboratory were crossed with *Nipp1* floxed animals generated as previously described [8]. C57BL6J mice were reared in standard housing conditions and given food/water ad libitum. All mouse experiments were conducted at P15–21 (mixed sex).

### Western Blotting and Antibodies

Mice were deeply anesthetized using a $CO_2$ before being euthanized by rapid decapitation. The brain was removed quickly, and different parts of the brain were rapidly dissected out on ice. The tissues were suspended in RIPA buffer and mechanically homogenized by using a polytron tissue homogenizer. Protein quantitation was performed using a BCA kit, and 20 μg of total protein was loaded for SDS-PAGE as performed previously [32]. Antibodies include anti-NIPP1 (1:1000; Sigma), anti-tubulin (1:2000; Chemi-con), anti-actin (1:4000; Sigma), anti-phospho-tau (S202, T205) (AT8) (1:500; Invitrogen), anti-p-tauThr231 (1:1000; Millipore), anti-tau (1:1000; Sigma), anti-PP1 pT320 (1:1000; Cell Signaling Technology), anti-PP1 (1:1000; E-9, Santa Cruz Biotechnology, Inc.), anti-pAKT (Ser473) (1:500; Cell Signaling), anti-AKT (1:1000; Cell Signaling), anti-pGSK3β (Ser9) (1:500; Cell Signaling), anti-GSK3β (1:1000; SCBT), anti-pERK1/2 (1:500; Cell Signaling), anti-pERK1/2 (1:1000; Cell Signaling), and anti-MBP (1:1000; Bio-Rad). Blots were

quantified using AzureSpot. For p-tau epitopes, the more prominent top band was used for analysis.

## Electron Microscopy

Optic nerves were immersion fixed in a combination fixative containing 2.0% paraformaldehyde/2.5% glutaraldehyde + 0.5% sucrose in 0.1 M sodium cacodylate buffer (pH 7.4). After 24 h of primary fixation, the nerves were rinsed in the same buffer and post-fixed for 2 h in buffered 1.0% osmium tetroxide/1.5% potassium ferrocyanide, washed in distilled water, dehydrated in a graded series of ethanol to 100% (× 3), transitioned into propylene oxide, infiltrated with EPON/Araldite resin overnight, embedded into molds, and polymerized for 48 h at 60 °C. The blocks were sectioned at 1 μm and stained with toluidine blue prior to thin sectioning at 70 nm onto slot formvar/carbon-coated nickel grids. The grids were stained with aqueous uranyl acetate and lead citrate and examined using a Hitachi 7650 TEM with an attached Gatan 11 megapixel Erlangshen digital camera and DigitalMicrograph software. Images were analyzed with *FIJI*, and *g*-ratios were calculated using an *ImageJ* plug-in (available at http://gratio.efil.de/), from randomly selected axons. *G*-ratios were calculated using the inner myelin sheath diameter (as opposed to the axon diameter, to avoid skewing data from potentially abrogated inner myelin tongues) divided by the outer myelin sheath diameter. Circumferences were manually traced.

## Electrophysiology

For complete details, see [33]. Briefly, mice were euthanized with $CO_2$, and optic nerves were dissected and placed in oxygenated artificial cerebral spinal fluid (ACSF) for 1 h at room temperature. ACSF contained 125 mM NaCl, 1.25 mM $NaH_2PO_4$, 25 mM D-glucose, 25 mM $NaHCO_3$, 2.5 mM $CaCl_2$, 1.3 mM $MgCl_2$, and 2.5 mM KCl and was bubbled with 95% $O_2$/5% $CO_2$. Nerves were transferred to a temperature-controlled chamber and perfused with ACSF. Each end of a nerve was drawn into a suction electrode for stimulation (at the retinal end) and recording. The stimuli were applied at 50 μsec duration and with supramaximal current amplitudes. CAP records were low-pass filtered at 10 kHz and fed into a data processing system for later analysis.

## Immunohistochemistry

Mice were deeply anesthetized using a combination of ketamine/xylazine. Animals were then transcardially perfused with PBS followed by 4% paraformaldehyde (PFA). Brains were carefully excised and placed in 4% PFA overnight at 4 °C. Brains were then rinsed with PBS and sunk in 30% sucrose in PBS at 4 °C. Brains were then carefully snap frozen in liquid nitrogen and then placed in block molds containing optimal cutting temperature (OCT) compound. Cryosections were then cut at 16 μm at − 17 °C. Sections were allowed to dry at room temperature overnight. Sections were then washed with PBS and placed in Liberate Antibody Binding (L.A.B. Polysciences Inc.) solution for 5 min. Sections were then washed 3 × with PBS and incubated in 0.5% Triton in PBS at 37 °C for 30 min. Slides were then washed 3 × with PBS. Five percent of donkey serum in PBS was then used to block the sections for 1 h. Primary antibodies, ASPA (1:100; Genetex), or Olig-2 (1:100; Millipore) were added, and slides were incubated at 37 °C for 1 h and then held overnight at 4 °C. Slides were then washed with PBS and incubated for 1 h at room temperature with

Alexa 488 donkey anti-rabbit antibody (1:400, in 5% donkey serum). DAPI was used to label nuclei. Thoroughly washed slides were mounted and allowed to dry overnight before imaging on the Keyence BZ-X800 fluorescent microscope. Images were randomized using a plug-in for *ImageJ* (https://imagej.nih.gov/ij/macros/Filename_Randomizer.txt), and the corpus callosum of each image was carefully traced by hand. Only cells within that region of interest were then counted.

### Statistical Analyses

The Shapiro–Wilk normality test was applied to verify normality of data. Unpaired two-tailed *t*-tests with alpha set to 0.05 were applied to parametric data to compare the differences between two groups. The Mann–Whitney *U* test was applied for sets where both groups rejected the null hypothesis of the Shapiro–Wilk test. The averages were denoted as mean ± SEM in all bar graphs. All statistical tests were performed using *GraphPad Prism9.3* software.

## Acknowledgements

We thank the technical help of Karen Bentley, director of Electron Microscopy Core of URMC, and Drs. Mathieu Bollen and Aleyde Van Eynde (KU Leuven, Belgium) for providing the floxed NIPP1 mice in our study.

### Funding

This work is supported by the National Institutes of Health (NIH) (R01 MH109719) and the National Science Foundation (NSF) (IOS-1457336) to HX and the NIH (F30 MH122046) to KF.

## Data Availability

The datasets generated during and/or analyzed during the current study are available from the corresponding author on reasonable request.

## References

1. Trinkle-Mulcahy L, Ajuh P, Prescott A, Claverie-Martin F, Cohen S, Lamond AI, Cohen P (1999) Nuclear organisation of NIPP1, a regulatory subunit of protein phosphatase 1 that associates with pre-mRNA splicing factors. J Cell Sci 112(Pt 2):157–168 [PubMed: 9858469]
2. Winkler C, Rouget R, Wu D, Beullens M, Van Eynde A, and M (2018) Bollen, *Overexpression of PP1-NIPP1 limits the* capacity *of cells to repair DNA double-strand breaks*. J Cell Sci 131(13).
3. Ferreira M, Verbinnen I, Fardilha M, Van Eynde A, Bollen M (2018) The deletion of the protein phosphatase 1 regulator NIPP1 in testis causes hyperphosphorylation and degradation of the histone methyltransferase EZH2. J Biol Chem 293(47):18031–18039 [PubMed: 30305391]
4. Jin Q, van Eynde A, Beullens M, Roy N, Thiel G, Stalmans W, Bollen M (2003) The protein phosphatase-1 (PP1) regulator, nuclear inhibitor of PP1 (NIPP1), interacts with the polycomb group protein, embryonic ectoderm development (EED), and functions as a transcriptional repressor. J Biol Chem 278(33):30677–30685 [PubMed: 12788942]
5. Minnebo N, Gornemann J, O'Connell N, Van Dessel N, Derua R, Vermunt MW, Page R et al. (2013) NIPP1 maintains EZH2 phosphorylation and promoter occupancy at proliferation-related target genes. Nucleic Acids Res 41(2):842–854 [PubMed: 23241245]
6. Van Dessel N, Beke L, Gornemann J, Minnebo N, Beullens M, Tanuma N, Shima H, Van Eynde A, Bollen M (2010) The phosphatase interactor NIPP1 regulates the occupancy of the histone methyltransferase EZH2 at Polycomb targets. Nucleic Acids Res 38(21):7500–7512 [PubMed: 20671031]

7. Van Eynde A, Nuytten M, Dewerchin M, Schoonjans L, Keppens S, Beullens M, Moons L, Carmeliet P, Stalmans W, Bollen M (2004) The nuclear scaffold protein NIPP1 is essential for early embryonic development and cell proliferation. Mol Cell Biol 24(13):5863–5874 [PubMed: 15199142]
8. Boens S, Verbinnen I, Verhulst S, Szeker K, Ferreira M, Gevaert T, Baes M, Roskams T et al. (2016) Brief report: the deletion of the phosphatase regulator NIPP1 causes progenitor cell expansion in the adult liver. Stem Cells 34(8):2256–2262 [PubMed: 27068806]
9. Ferreira M, Boens S, Winkler C, Szeker K, Verbinnen I, Van Eynde A, Fardilha M, Bollen M (2017) The protein phosphatase 1 regulator NIPP1 is essential for mammalian spermatogenesis. Sci Rep 7(1):13364 [PubMed: 29042623]
10. Verbinnen I, Jonkhout M, Liakath-Ali K, Szeker K, Ferreira M, Boens S, Rouget R, Nikolic M et al. (2020) Phosphatase regulator NIPP1 restrains chemokine-driven skin inflammation. J Invest Dermatol 140(8):1576–1588 [PubMed: 31972250]
11. Novoyatleva T, Heinrich B, Tang Y, Benderska N, Butchbach ME, Lorson CL, Lorson MA, Ben-Dov C et al. (2008) Protein phosphatase 1 binds to the RNA recognition motif of several splicing factors and regulates alternative pre-mRNA processing. Hum Mol Genet 17(1):52–70 [PubMed: 17913700]
12. Welden JR, van Doorn J, Nelson PT, Stamm S (2018) The human MAPT locus generates circular RNAs. Biochim Biophys Acta Mol Basis Dis 1864(9):2753–2760 [PubMed: 29729314]
13. Wang Y, Mandelkow E (2016) Tau in physiology and pathology. Nat Rev Neurosci 17(1):5–21 [PubMed: 26631930]
14. Braithwaite SP, Stock JB, Lombroso PJ, Nairn AC (2012) Protein phosphatases and Alzheimer's disease. Prog Mol Biol Transl Sci 106:343–379 [PubMed: 22340724]
15. Readhead C, Hood L (1990) The dysmyelinating mouse mutations shiverer (shi) and myelin deficient (shimld). Behav Genet 20(2):213–234 [PubMed: 1693848]
16. Hou H, Sun L, Siddoway BA, Petralia RS, Yang H, Gu H, Nairn AC, Xia H (2013) Synaptic NMDA receptor stimulation activates PP1 by inhibiting its phosphorylation by Cdk5. J Cell Biol 203(3):521–535 [PubMed: 24189275]
17. Mayoral SR, Etxeberria A, Shen YA, Chan JR (2018) Initiation of CNS myelination in the optic nerve is dependent on axon caliber. Cell Rep 25(3):544–550 (e3) [PubMed: 30332636]
18. Yang H, Hou H, Pahng A, Gu H, Nairn AC, Tang YP, Colombo PJ, Xia H (2015) Protein phosphatase-1 inhibitor-2 is a novel memory suppressor. J Neurosci 35(45):15082–15087 [PubMed: 26558779]
19. Dickson DW, Kouri N, Murray ME, Josephs KA (2011) Neuropathology of frontotemporal lobar degeneration-tau (FTLD-tau). J Mol Neurosci 45(3):384–389 [PubMed: 21720721]
20. Saab AS, Tzvetavona ID, Trevisiol A, Baltan S, Dibaj P, Kusch K, Mobius W, Goetze B et al. (2016) Oligodendroglial NMDA receptors regulate glucose import and axonal energy metabolism. Neuron 91(1):119–132 [PubMed: 27292539]
21. McKenzie IA, Ohayon D, Li H, de Faria JP, Emery B, Tohyama K, Richardson WD (2014) Motor skill learning requires active central myelination. Science 346(6207):318–322 [PubMed: 25324381]
22. Monje M (2018) Myelin plasticity and nervous system function. Annu Rev Neurosci 41:61–76 [PubMed: 29986163]
23. Birey F, Kloc M, Chavali M, Hussein I, Wilson M, Christoffel DJ, Chen T, Frohman MA et al. (2015) Genetic and stress-induced loss of NG2 glia triggers emergence of depressive-like behaviors through reduced secretion of FGF2. Neuron 88(5):941–956 [PubMed: 26606998]
24. Fields RD (2008) White matter in learning, cognition and psychiatric disorders. Trends Neurosci 31(7):361–370 [PubMed: 18538868]
25. Raabe FJ, Slapakova L, Rossner MJ, Cantuti-Castelvetri L, Simons M, Falkai PG, and Schmitt A (2019) Oligodendrocytes as a new therapeutic target in schizophrenia: from histopathological findings to neuron-oligodendrocyte interaction. Cells, 8(12).
26. Lee S, Leach MK, Redmond SA, Chong SY, Mellon SH, Tuck SJ, Feng ZQ, Corey JM, Chan JR (2012) A culture system to study oligodendrocyte myelination processes using engineered nanofibers. Nat Methods 9(9):917–922 [PubMed: 22796663]

27. Bonetto G, Kamen Y, Evans KA, Karadottir RT (2020) Unraveling myelin plasticity Front Cell Neurosci 14:156 [PubMed: 32595455]

28. Demerens C, Stankoff B, Logak M, Anglade P, Allinquant B, Couraud F, Zalc B, Lubetzki C (1996) Induction of myelination in the central nervous system by electrical activity. Proc Natl Acad Sci U S A 93(18):9887–9892 [PubMed: 8790426]

29. Gibson EM, Purger D, Mount CW, Goldstein AK, Lin GL, Wood LS, Inema I, Miller SE et al. (2014) Neuronal activity promotes oligodendrogenesis and adaptive myelination in the mammalian brain. Science 344(6183):1252304 [PubMed: 24727982]

30. Mitew S, Gobius I, Fenlon LR, McDougall SJ, Hawkes D, Xing YL, Bujalka H, Gundlach AL et al. (2018) Pharmacogenetic stimulation of neuronal activity increases myelination in an axon-specific manner. Nat Commun 9(1):306 [PubMed: 29358753]

31. Goebbels S, Wieser GL, Pieper A, Spitzer S, Weege B, Yan K, Edgar JM, Yagensky O et al. (2017) A neuronal PI(3,4,5) P3-dependent program of oligodendrocyte precursor recruitment and myelination. Nat Neurosci 20(1):10–15 [PubMed: 27775720]

32. Siddoway B, Hou H, Yang J, Sun L, Yang H, Wang GY, Xia H (2014) Potassium channel Kv2.1 is regulated through protein phosphatase-1 in response to increases in synaptic activity. Neurosci Lett 583:142–7 [PubMed: 25220706]

33. Shrager P, Youngman M (2017) Preferential conduction block of myelinated axons by nitric oxide. J Neurosci Res 95(7):1402–1414 [PubMed: 27614087]

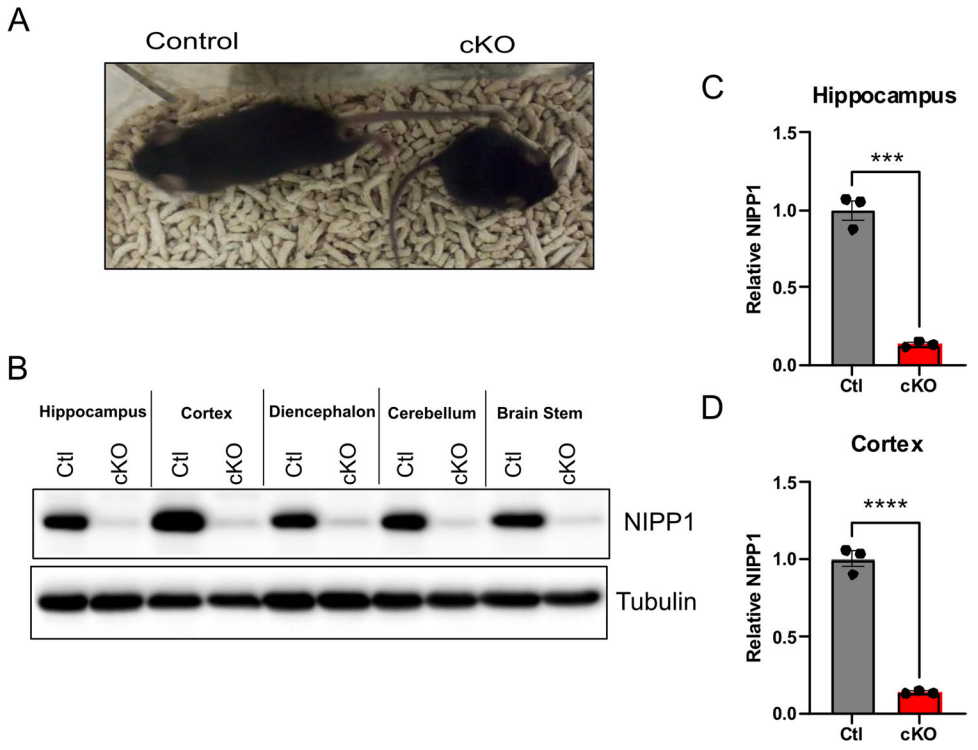


**Fig. 1.**

NIPP1 cKO mice are smaller than littermate controls. **A** Image of control mouse (left) with NIPP1 cKO littermate (right). **B** Representative western blot of CNS tissues probed for NIPP1. **C** Quantification of relative NIPP1 levels in hippocampal tissue normalized to tubulin (two-tailed unpaired *t*-test; $p = 0.0002$, $n = 3$ animals). **D** Quantification of relative NIPP1 levels in cortical tissue normalized to tubulin (two-tailed unpaired *t*-test; $p < 0.0001$, $n = 3$ animal pairs). Data are mean ± SEM; *$p < 0.05$, **$p < 0.01$, ***$p < 0.001$, ****$p < 0.0001$

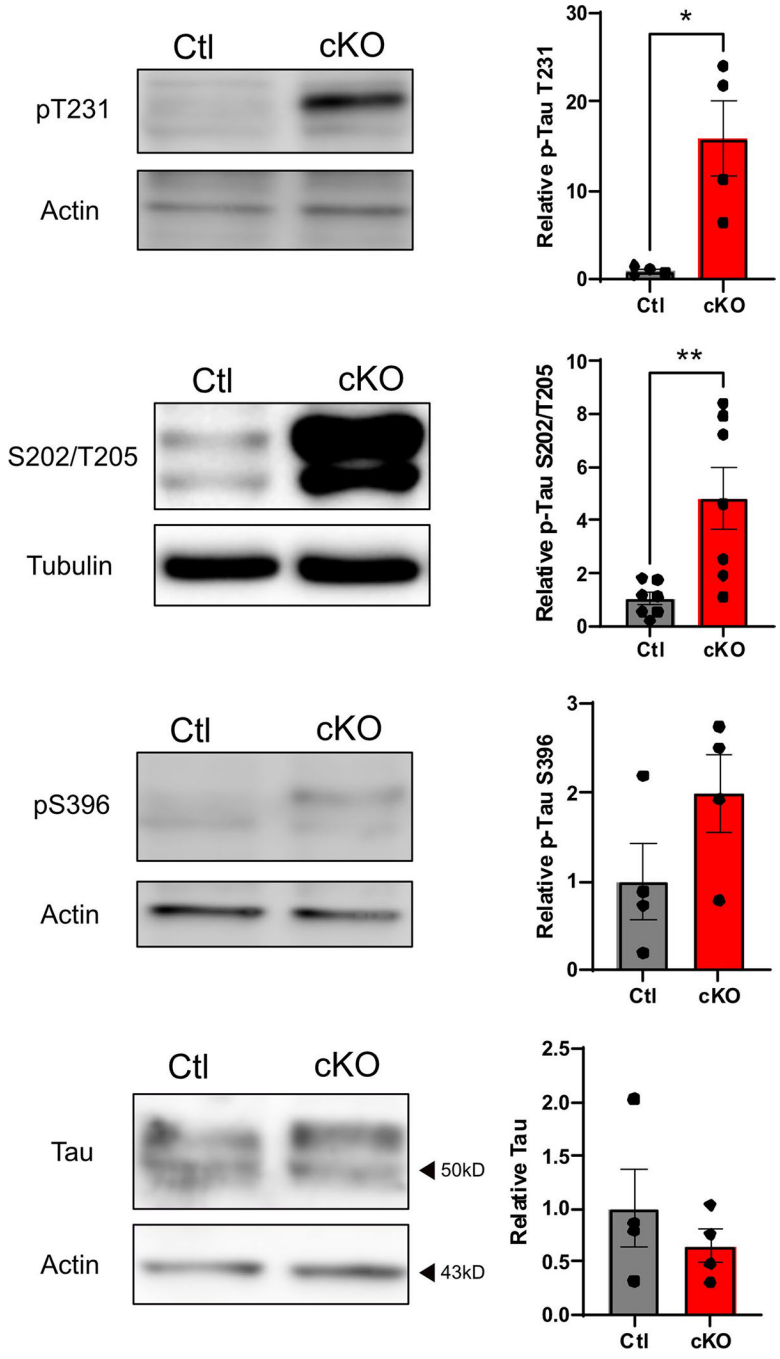


**Fig. 2.**

Increased tau phosphorylation in the NIPP1 cKO mouse cortex. Western blot of cortical tissue from NIPP1 cKO mice probed with various antibodies specific for phospho-tau epitopes and total tau (left) with respective quantifications (right). Phospho-tau epitopes were quantified using the top prominent band and normalized to actin or tubulin. Significant differences observed for p-tau T231 (two-tailed unpaired *t*-test; $p = 0.0122$, $n = 4$ animal pairs) and S202/T205 (two-tailed unpaired *t*-test; $p = 0.0073$, $n = 7$ animal pairs). No significant difference detected for p-tau S396 (two-tailed unpaired *t*-test; $p = 0.1553$, $n = 4$

animal pairs) or total tau (two-tailed unpaired *t*-test; $p = 0.406$, $n = 4$ animal pairs). Data are mean ± SEM; *$p < .05$, **$p < 0.01$

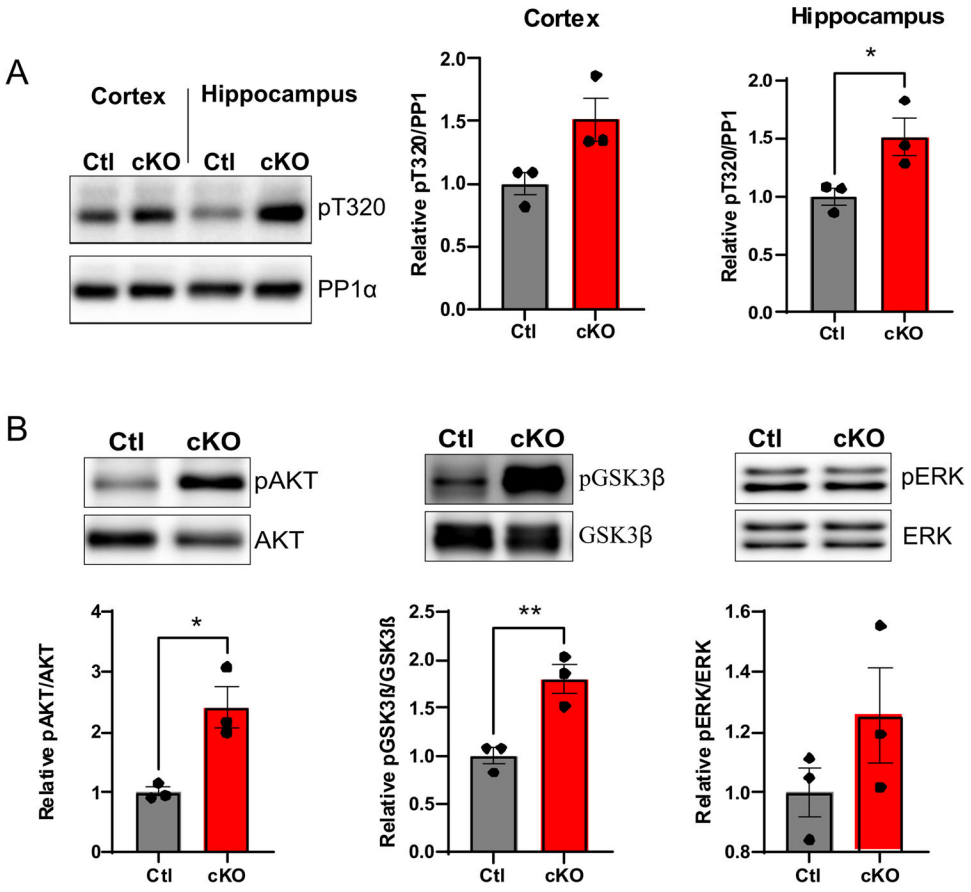


**Fig. 3.**

Altered activity of tau phosphatase and kinases in NIPP1 cKO mice. **A** Western blot probed for inhibitory (pT320) PP1 epitope (left) along with quantification in the cortex (Mann–Whitney test; $p = 0.1$) and hippocampus (two-tailed unpaired *t*-test; $p = 0.0437$, $n = 3$ animal pairs) (right). **B** Western blot of cortical tissue probed for various known tau kinases (left) along with quantifications (relative pAKT; two-tailed unpaired *t*-test; $p = 0.0153$, $n = 3$ animal pairs; relative pGSK3β; two-tailed unpaired *t*-test; $p = 0.0097$, $n = 3$ animal pairs; relative pERK; two-tailed unpaired *t*-test; $p = 0.2260$, $n = 3$ animal pairs) (right). Data are mean ± SEM; $*p < 0.05$, $**p < 0.01$

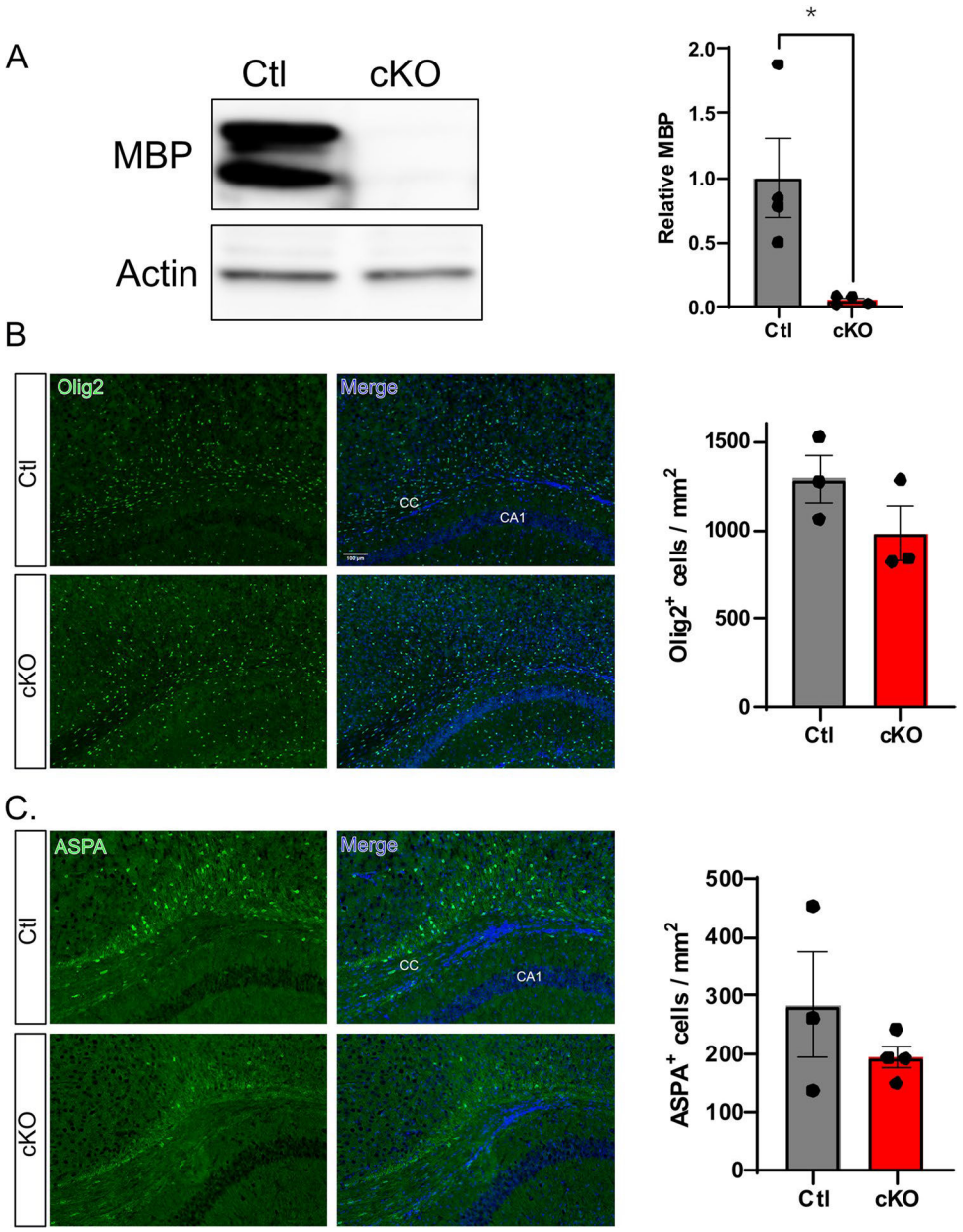


**Fig. 4.**

Myelin basic protein (MBP) level is decreased, without a change in OPC/OL densities, in NIPP1 cKO mice. **A** Representative western blot of cortical tissue from NIPP1 cKO mice with littermate controls probed for MBP (left) along with quantification (two-tailed unpaired *t*-test; $p = 0.0204$; $n = 3$ animal pairs) (right). **B** Immunostaining of brain sections from control and NIPP1 cKO mice stained with pan-oligodendrocyte marker, Olig2, and merged with DAPI (left). Quantification of Olig2 in the corpus callosum (two-tailed unpaired *t*-test; $p = 0.2052$; $n = 3$ animal pairs) (right). **C** Immunostaining of brain sections from control and NIPP1 cKO mice stained with mature oligodendrocyte marker, ASPA, and merged with DAPI (left). Quantification of ASPA in the corpus callosum (two-tailed unpaired *t*-test; $p = 0.3153$; Ctl animals = 3, cKO animals = 4) (right). Data are mean ± SEM

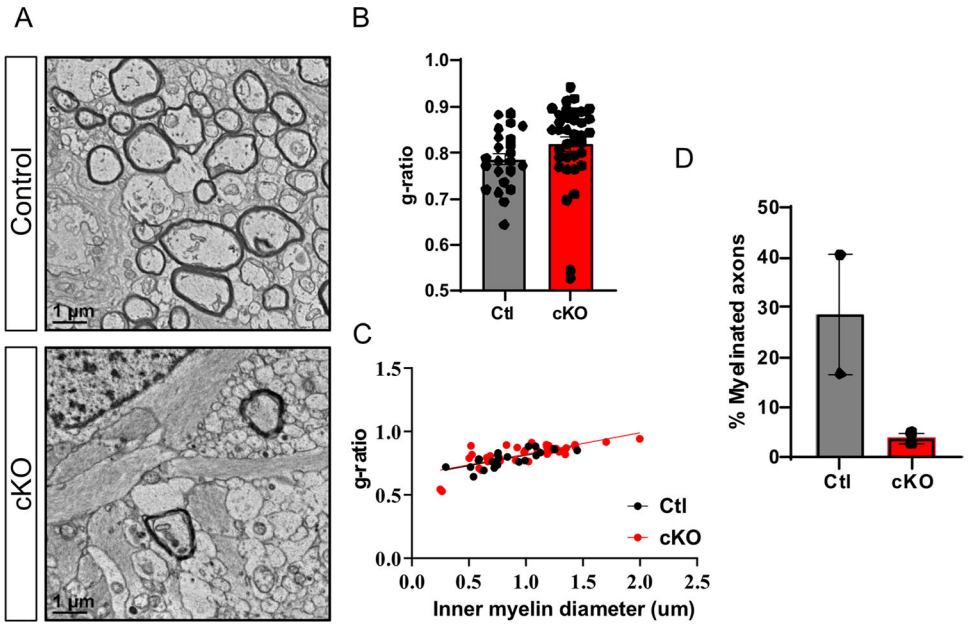


**Fig. 5.**

Myelin deficits in the optic nerve of NIPP1 cKO mice. **A** Representative electron micrographs of optic nerve cross sections from control and NIPP1 cKO animals, respectively. **B** mean *g*-ratio of myelinated axons calculated from the inner myelin diameter/outer myelin diameter (two-tailed unpaired *t*-test; $p = 0.1168$, control axons = 23; cKO axons = 36, animal pairs = 2). **C** *g*-ratios plotted as a function of axon diameter, overlaid with lines of best fit. **D** Percentage of myelinated axons. Data are mean ± SEM

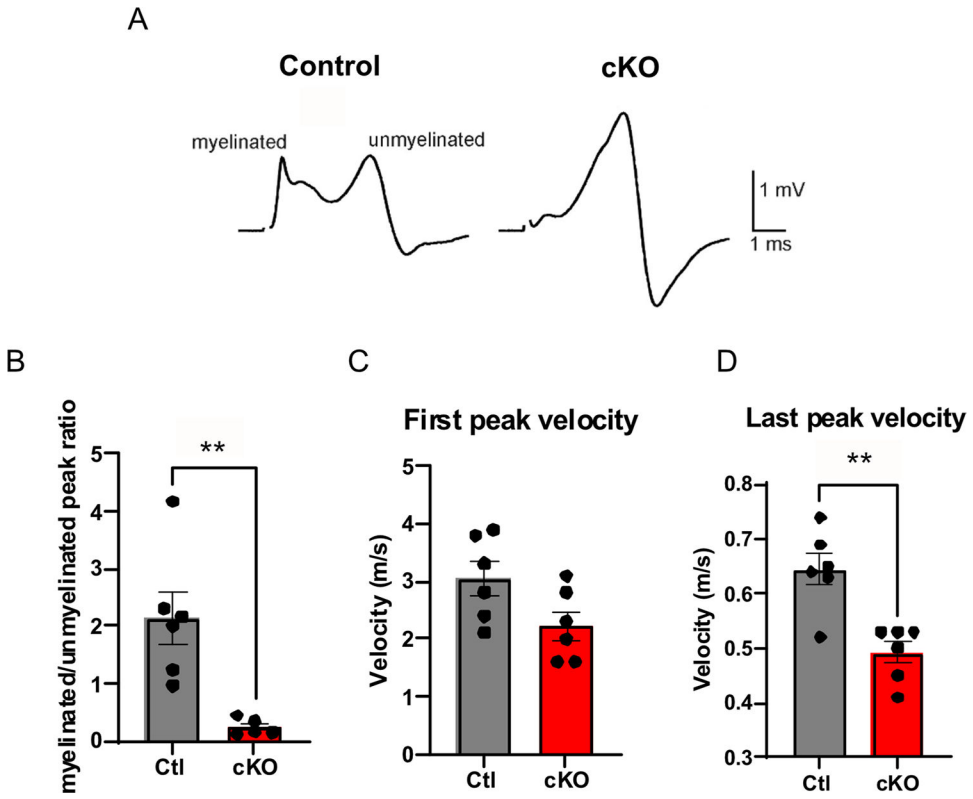


**Fig. 6.**

Compound action potential deficits in the NIPP1 cKO mouse optic nerve. Compound action potentials from control (left) and cKO (right) optic nerves. **A** Representative traces with stimulus artifacts removed for clarity. In each trace, the faster (first) peak represents myelinated axons, and the slower peak unmyelinated (pre-myelinated) axons. **B** Ratio of myelinated/unmyelinated peaks (two-tailed unpaired *t*-test; $p = 0.0048$). **C**–**D** Calculated velocities of the first (two-tailed unpaired *t*-test; $p = 0.0653$) and last peaks (two-tested unpaired *t*-test; $p = 0.0018$), respectively. Ctl nerves = 6, cKO nerves = 5, animal pairs = 3. Data are mean ± SEM; *$p < 0.05$, **$p < 0.01$